Three-dimensional analysis of creep voids in copper by serial sectioning combined with large field EBSD

Ramin Abbasi, Kristof Dzieciol, András Borbély

▶ **To cite this version:**

Ramin Abbasi, Kristof Dzieciol, András Borbély. Three-dimensional analysis of creep voids in copper by serial sectioning combined with large field EBSD. Materials Science and Technology, 2015, 31 (Issue : 5), pp.540-546. 10.1179/1743284714Y.0000000593 . emse-01498677

HAL Id: emse-01498677

https://hal-emse.ccsd.cnrs.fr/emse-01498677v1

Submitted on 22 Apr 2024

HAL is a multi-disciplinary open access archive for the deposit and dissemination of scientific research documents, whether they are published or not. The documents may come from teaching and research institutions in France or abroad, or from public or private research centers.

L'archive ouverte pluridisciplinaire **HAL**, est destinée au dépôt et à la diffusion de documents scientifiques de niveau recherche, publiés ou non, émanant des établissements d'enseignement et de recherche français ou étrangers, des laboratoires publics ou privés.

Three-dimensional analysis of creep voids in copper by serial sectioning combined with large field EBSD

R. Abbasi, K. Dzieciol and A. Borbély*

The three-dimensional granular and damage structure of two creep deformed copper specimens has been reconstructed using an improved serial sectioning method combining optical profilometry, scanning electron imaging and backscatter electron diffraction. The reconstructions permitted associating creep voids to grain boundaries and evaluating the damage probability of each grain boundary type. The results indicate that creep damage of oxygen free high conductivity copper is governed by topological factors. Quadruple/grain boundaries have the highest probability of damage followed by two- and three-grain boundaries with decreasing percentages. The damage probability of quadruple and three-grain boundaries increases with decreasing stress due to a larger contribution of grain boundary sliding to void nucleation. The relative frequency of damaged two-grain boundaries increases with stress, suggesting a significant role of creep plasticity and the associated grain boundary ledges. No correlation between void location and the crystallographic orientation of neighbour grains was found.

Keywords: Creep damage, Serial sectioning, EBSD, 3D reconstruction

Introduction

The lifetime of engineering components exposed to high temperature creep is generally limited by the nucleation and growth of intergranular voids. In-service problems led to the topic being extensively studied 30–40 years ago,[1–3] but due to the lack of adequate experimental techniques the understanding of the three-dimensional (3D) character of damage, closely related to void topology, remained limited.[4] With the advent of powerful synchrotron sources and novel tomography techniques with resolution below the micrometre, there has been a revival of creep damage studies.[5,6] Through the determination of real 3D quantities, such as void volume, interconnectivity and spatial arrangement, synchrotron X-ray tomography provided new insight into this interesting phenomenon.[7–10] Furthermore, the non-destructive nature of the technique permitted for the first time the experimental validation[11,12] of the viscous type void-growth law predicted by Budiansky *et al.*[13] *In situ* tomography studies have shown that while void growth during power law creep has indeed a viscous character, the real growth rates in copper[11] and in brass[12] are larger by one order of magnitude than the prediction of the non-linearly viscous continuum model.[13] The discrepancy between experiment and model lies evidently in the approximation of the polycrystalline structure as a homogeneous media, which is inappropriate to quantitatively describe void growth at a grain boundary (GB) since it neglects the crystalline nature of the grains and the local topology. Since absorption tomography is insensitive to crystallographic orientation, topological aspects such as the location of creep voids at different GB types is missing from the analysis. Therefore, further exploration of the subject requires techniques sensitive to crystallographic orientation.

Various methods have been developed for capturing the polycrystal structure, which can be classified according to their destructive or non-destructive nature. The simplest destructive technique is serial sectioning, based on the gradual removal of material layers to obtain a series of surfaces suitable for microscopy (by optical or by scanning electron microscopy, SEM) and from which a 3D image [a stack of two-dimensional (2D) images] can be created. Once the dataset acquired, the volume can be reconstructed using image processing. Serial sectioning permits generation of significantly large volumes (about few mm^3) at relatively high resolution (down to submicrometric) and has been used for over a century in different scientific fields such as mineralogy[14] and biology,[15] but only since the end of the 20th century in materials science.[16–18] Non-destructive imaging techniques are relatively recent and are being developed at synchrotron sources.[19] These include diffraction contrast tomography[20] and high energy diffraction microscopy,[21] which are capable of reconstructing polycrystalline volumes as large as one cubic millimetre with a spatial resolution of about one micrometre. Both techniques

Ecole Nationale Supérieure des Mines, SMS-EMSE, CNRS:UMR 5307, LGF, 42023, Saint-Etienne Cedex 2, France

*Corresponding author, email borbely@emse.fr

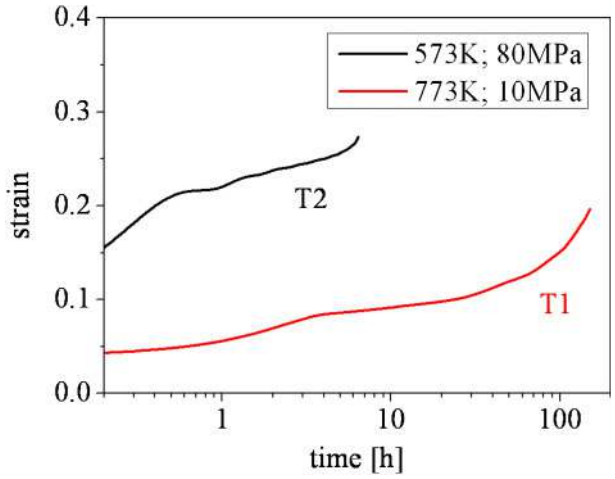

1 Creep curves of oxygen free high conductivity copper under T1 and T2 loading conditions

work well with non-deformed materials, but they cannot be yet applied to deformed polycrystals. Therefore, creep damage studies have, until today, only been performed with the serial sectioning technique[22,23] as is also the case in the present work. The question we address concerns the influence of void's GB topology [such as two, three and four-grain boundary type (2GB, 3GB and 4GB respectively)] and of crystallographic orientation of neighbour grains (described in terms of the highest Schmid factor) on the power law creep damage of pure copper.

Experimental procedure

Material and creep deformation

Creep tests were performed on specimens made of oxygen free high conductivity copper with a laboratory developed device using constant load conditions. Dog bone shaped samples with dimensions of 1·8 mm in diameter and 4 mm gauge length were placed into a quartz tube with a good vacuum of 10^{-4}–10^{-5} Pa supplied by a coupled system of rotary and turbomolecular pumps. The load was applied at the exterior of the tube via a metal bellows closing element connected to the sample with self-aligning load–train couplers assuring a uniaxial stress state. Stress concentrations at the ends of the gauge length were avoided by using conical sample heads. Specimen elongation was obtained by measuring the displacement of the bellows. Two loading conditions were applied. The first test (T1) was done at a temperature of 773 K and a stress of 10 MPa, while the second (T2) at lower temperature but higher stress (573 K, 80 MPa). The stress values correspond to the initial state when the load was applied. The creep curves of the two specimens are shown in Fig. 1 and indicate that the analysed deformation states correspond to the beginning of the tertiary creep regime. The minimum creep rates under T1 and T2 deformation conditions were 2×10^{-7} and 1×10^{-6} s^{-1}, respectively. According to the approximate deformation mechanism maps of Frost and Ashby,[24] both conditions are located in the power law creep region of copper. T1 is nearer to the diffusional flow, while T2 to the power law breakdown region. Therefore, one expects that deformation of sample T1 is more influenced by diffusion creep, while that of T2 by plasticity. Furthermore, it is expected that grain boundary sliding (GBS) will have an increased contribution in sample T1 compared to T2, as it is suggested by the corresponding minimum creep rate equation. In the case of grain boundary sliding, the stress exponent is generally smaller than for dislocation creep.[25]

Improved reconstruction method based on serial sectioning

The granular structure and damage of the crept specimens was reconstructed using an improved serial sectioning technique combining several instruments.[26] Compared to the conventional method consisting of material removal and optical microscopy or SEM imaging, the present approach included two additional steps permitting (1) the measurement of the removed material thickness with the help of a profilometer and (2) the characterisation of the crystallographic orientation of the grains by electron backscatter diffraction (EBSD). Material removal was performed using the Chemical–mechanical planarisation technique that is now routinely applied in the microelectronic industry.[27] The slurry used in this work was the STRUERS OP-S suspension with a pH of 9·8 and a grain size of about 40 nm. chemical–mechanical planarisation was performed on a LAMPLAN Mastertex polishing cloth designed for small colloidal particles. Optimised polishing conditions were obtained at a rotation of 400 rev min^{-1} and a stress of 0·1 MPa on the sample. The total thickness of the removed material was of about 40 μm, somewhat larger than the mean grain size. Polishing was done in 37 steps resulting in a mean removal rate of $1{\cdot}1 \pm 0{\cdot}56$ μm per layer. After the first polishing step, a rectangular region of interest with area of about $1 \times 0{\cdot}8$ mm was selected on the longitudinal section (parallel to the applied load axis) of the samples and marked with four indents placed at its corners. The region of interest was characterised as follows:

(i) the polished surface was first scanned with an optical profilometer (Weeko NT9100) to calculate the removed local material thickness as the difference between two consecutive layer scans. The reference points for this comparison were the tips of the indents unaffected by polishing. This additional step avoids the requirement of parallel polished sections and gives the local thickness of the removed layer with an accuracy of 0·5 μm in vertical direction. The lateral resolution of the profilometer image was 0·37 μm. This was later reduced by interpolation to 0·5 μm

(ii) the second step consists in imaging the polished surface using backscatter electrons (BSEs) using a Supra 55VP ZEISS SEM. The good contrast of these images (Fig. 2*a*) allowed easy segmentation of the voids. BSE imaging was performed after each polishing step and since these images had the highest quality they were used as the basis for the 3D reconstruction. The vertical coordinate associated with each image pixel was obtained by registering BSE and profilometer images. To perform the registration, the pixel size of the BSE image was reduced to 0·5 μm by linear interpolation. Therefore, the final reconstructed 3D image of damage had a voxel size of 0·5 μm (as determined by the vertical resolution of the profilometer optics)

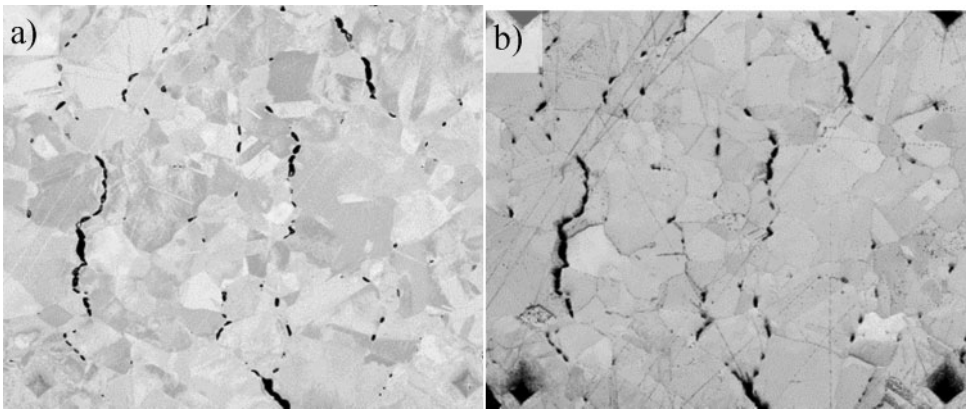

a BSE image; *b* EBSD band contrast image

2 Damage structure of copper sample deformed under T1 conditions

(iii) the final step concerns the determination of the crystallographic orientation of the grains by EBSD. Since the analysis area ($1 \times 0{\cdot}8$ mm) was large, EBSD acquisition was performed in cartography mode of the acquisition software (HKL Channel 5) using a scanning step size of 1 μm. The spatial resolution of the orientation information perpendicular to the scanned surface was, however, smaller, since EBSD scans were performed only after the removal of material layers of about 4–5 μm in thickness. EBSD maps were first enlarged to images with a pixel size of 0·5 μm and then registered with BSE images. For registration the band contrast EBSD image (Fig. 2*b*) was used, which showed a very good similarity with the corresponding BSE image (Fig. 2*a*). The crystallographic orientation of the grains was characterised by two quantities: (1) the average orientation and (2) the mean disorientation spread. The first can be related to the preferential activation of glide systems through the highest Schmid factor, while the second to the density of geometrically necessary dislocations (GNDs) in each grain.

Results

The influence of grain topology

Based on the work of Garboczi,[28] it is known that about 125 voxels are necessary to reasonably approximate the shape of an ellipsoidal particle. According to this criterion, only voids having a volume larger than 125 voxels were considered in the statistics. This resulted finally in 535 and 584 voids for samples deformed under T1 and T2 conditions respectively (shown in Fig. 3). In addition to smaller voids, both images indicate the existence of small cracks lying perpendicular to the direction of the applied load marked by horizontal arrows. These cracks as well as voids extending over a distance larger than the grain size were not taken into account in the evaluations.

Owing to time consuming EBSD scans (of about 8 h, with Nordlys detector) only volumes with a height of 40 μm were reconstructed. As an example, the resulting granular structure of the sample deformed under T1 condition is shown in Fig. 4*a*. It has a mean sphere equivalent (sphere with the same volume as the void) diameter of about 30 μm, which is somewhat smaller than the circle equivalent diameter of 40 μm determined form 2D EBSD maps. A better agreement between the 2D and 3D mean grain size was, however, found for the sample deformed under T2 conditions. The mean 3D grain size in this case was of about 35 μm. The analysis of the grain reconstruction permitted revealing the GBs, which were categorised in three groups: 2GBs, 3GBs and 4GBs. According to the quantitative results shown in Table 1, more GBs were identified in the T1 specimen in agreement with its lower average 3D grain size compared to the T2 sample.

Merging the grain structure obtained by EBSD with the 3D SEM image containing the voids allowed the classification of the latter according to the type of the GB they occupy. Voids were classified as: two-grain boundary voids (2GBV), three-grain boundary voids (3GBV) (Fig. 4*b*) and four-grain boundary voids (4GBV). According to Fig. 5*a*, the relative proportion of different void types is similar in both samples. The most numerous are the 2GBVs, followed by 3GBVs and 4GBVs. The relative frequency of 2GBVs is higher in the sample deformed under T2 conditions than T1. In both samples, however, the 3GBVs are larger than the 2GBVs

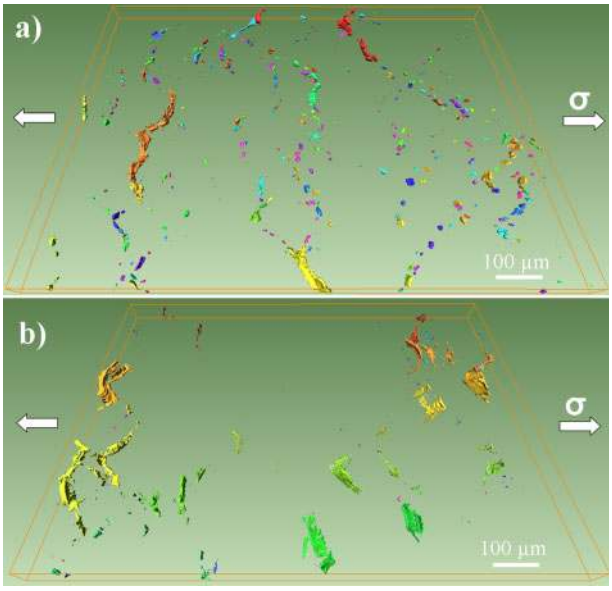

3 Perspective visualisation of creep voids in samples deformed under *a* T1 and *b* T2 conditions (Avizo software)

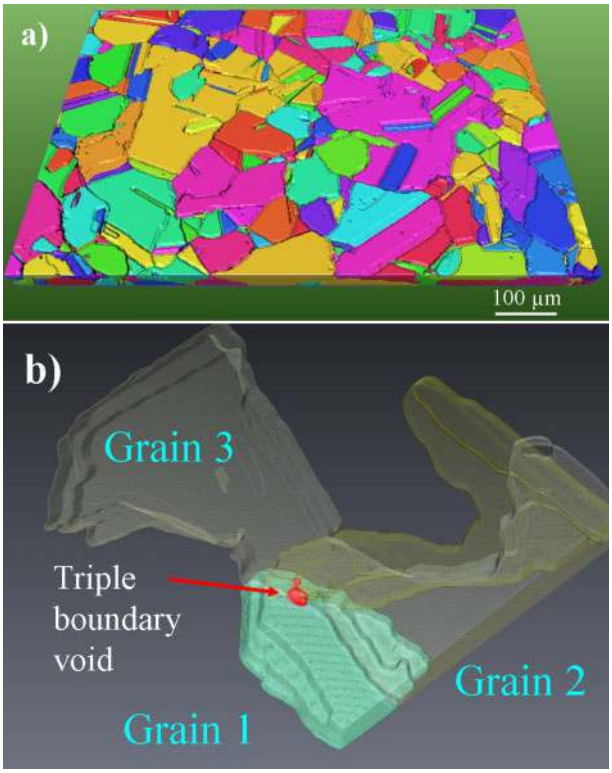

4 ***a*** **reconstructed granular structure of sample deformed at 773 K, 10 MPa (T1 condition) and** ***b*** **example of three-grain boundary void (3GBV) in sample deformed at 573 K, 80 MPa (T2 condition)**

as shown by the corresponding distributions of the void volume (Fig. 5*b*). In the case of the T1 sample, this has the consequence that the volume fraction of 3GBVs (0·124%) exceeds that of the 2GBVs (0·098%). The situation is reversed for sample T2, where 2GBVs are much more numerous and have a volume fraction of 0·029% compared to only 0·016% for 3GBVs.

The void topology enables one to relate GB to damage evolution. A GB was considered to be damaged if it contained one or more voids. The damage probability of a given GB type was calculated by dividing the number of damaged GBs of the selected type by the total number of GBs of the same type. Based on the results presented in Table 1, one can state that despite the different numbers of voids and GBs found, both specimens reveal a very high damage probability of the 4GBs (80–90%). This is followed in ranking by 2GBs and 3GBs, which show, however, significant differences between samples T1 and T2. Finding a 2GBV is more probable in the sample deformed at higher stress and lower temperature (T2), while 3GBVs are more probable during deformation at higher temperature and lower stress (T1).

Table 1 Total number of identified GBs N_T, number of GBs having void as neighbour N_V and relative frequency of GBs containing void R_f

	573 K, 80 MPa (T2)			773 K, 10 MPa (T1)		
GB type	2GB	3GB	4GB	2GB	3GB	4GB
N_T	1180	971	13	2723	2397	44
N_V	99	19	10	162	98	40
R_f/%	8·3	1·9	77	5·9	4·0	91

Influence of crystallographic orientation

The correlation between creep damage and crystallographic orientation was investigated by analyzing the Schmid factors of the primary slip system, the disorientation of neighbour grains and the mean disorientation spread of single grains. The aim was a comparison of these quantities for two grain populations: (1) all the grains available in the reconstruction and (2) grains containing a neighbouring void. The analysis yielded negative results regarding the influence of the Schmid factor and the disorientation of grains sharing a void. The distributions of Schmid factors for the two populations were found identical within the error of the evaluation (Fig. 6*a*). Similarly, the disorientation distribution of all neighbour grains was close to that of grain pairs sharing a pore and both were close to a Mckenzie distribution, characteristic of randomly oriented grains.[29] This near random disorientation distribution was also verified by grains sharing 2GBVs and 3GBVs, too (not shown). The disorientation of neighbour grains was calculated based on the average orientation of the reconstructed 3D grain, which is inherently affected by the positioning error of the analysed sample in the SEM–EBSD stage. Based on repeated measurements of the same sample section this error was estimated to be about 1–2°, which should not significantly change the distribution of the Schmid factors.

The third orientation parameter investigated was the mean disorientation spread (MDS) of each individual grain. In order to avoid the influence of sample repositioning, the MDS was separately calculated for each grain section and then a weighted average (according to the fraction of each section making up the 3D grain) over all sections was taken. Figure 6*b* compares the MDS distribution corresponding to all grains in the specimen with that of grains having a void as neighbour. A significant difference between the distributions was obtained. There is a greater probability of finding a grain with small MDS (below 2°) in the set of all grains making up the polycrystal, but a grain with large MDS (above 2°) is more probable among the set of damaged grains. As a consequence, grains with a neighbouring void have, on average, a higher GND density.

Discussion

An improved serial sectioning method has been applied to study power law creep damage in two copper specimens deformed under uniaxial stress. By coupling profilometry and SEM imaging, as well as EBSD characterisation, two different 3D volumes were generated: voids and grains. Merging the two reconstructions allowed relating voids with different GB types and the crystallographic orientation of the grains, so that different hypotheses on creep void nucleation can be checked.

Crystal plasticity finite element simulations indicate that at the boundary of a bicrystal, the resolved shear stress of the primary slip system in the harder grain is distinctly higher than that in the softer grain.[30] Assuming that voids nucleate already at the beginning

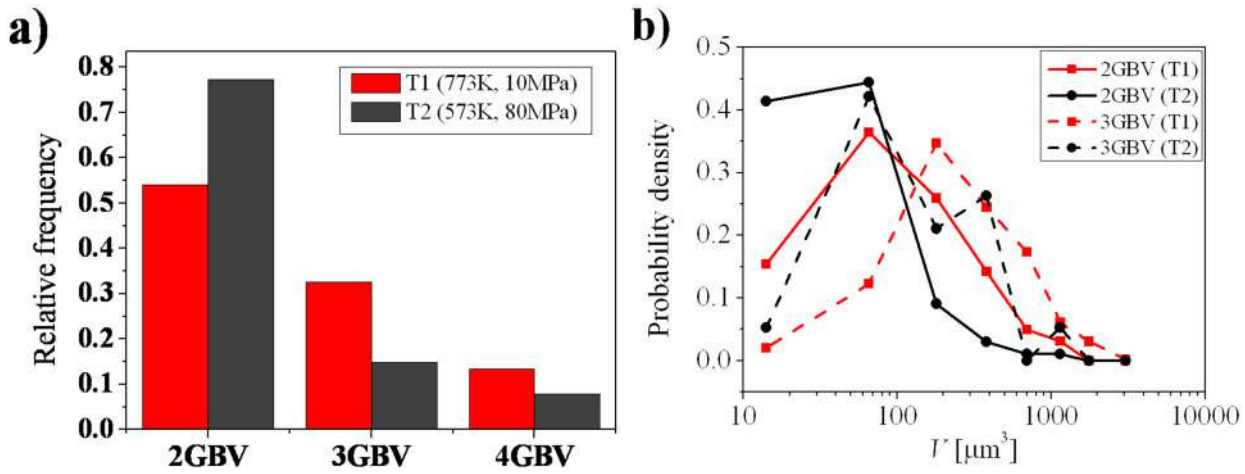

5 ***a*** **relative frequencies of different void types and** ***b*** **size distribution of 2GBVs and 3GBVs**

of the creep test[31] and that nucleation is determined by the local stress, one might expect a spatial correlation between voids and harder grains (with slips systems less favourably oriented for plastic slip). In other words, finding a void near a grain with a lower Schmid factor would be more probable than near a grain with a higher Schmid factor. The present analysis performed on about 1000 voids/grains did not confirm this hypothesis. The probability densities of the Schmid factor distribution for grains sharing a void and that for the total population of grains were found to be identical within the measurement error (Fig. 6*a*). This stress enhancement at the GB due to plastic anisotropy, which was found to influence the local plastic yield,[32] seems to have no effect on creep damage. Plastic slip, however, in terms of GND density, leads to preferential voids formation near grains with higher mean disorientation spread (Fig. 6*b*).

One important result of the present 3D analysis is related to the influence of GB topology on damage. 4GBs, where finding a creep void has the highest probability, seem to be the weakest points in the polycrystal. Less evident is the case of 3GBs with a relative frequency smaller than that of 2GBs. Based on thermodynamic and local stress equilibrium arguments Raj and Ashby[33] have shown that the free enthalpy of void formation is smaller at a 3GB than at a 2GB. The effect is related first of all to void topology, but might be further enhanced by the local stress, which is usually higher near a triple junction.[3] Based on these classical arguments, a higher relative frequency of 3GBVs compared to 2GBVs is expected, but in reality the opposite was found (Table 1). One possible way to reconcile experiment and theory is to consider more realistic conditions taking into account elastic anisotropy. Tvergaard and Hutchinson[34] have indeed shown that stress at a triple junction can be singular, but can also decay to zero. This behaviour depends on the degree of elastic anisotropies and the relative orientations of the crystal axes in the grains adjacent to the triple junction. Moreover, considering a power law creeping non-linearly viscous material, the stress singularity at a triple junction can relax rapidly,[35] which renders the task of theoretical prediction very difficult. As a consequence, the smaller relative frequency of 3GBVs compared to 2GBVs is not surprising and drawing a conclusion on the role of local stress in void nucleation requires a separate study for each cavity by taking into account their actual geometry and crystallographic orientation.

The present results are in agreement with the assumption that voids in pure metals nucleate preferentially at

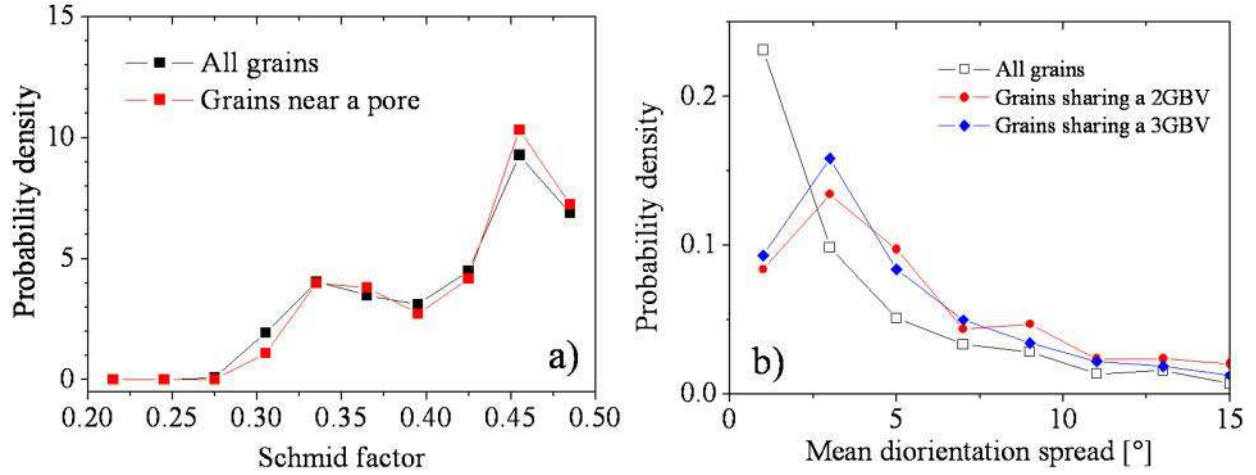

6 ***a*** **distribution of Schmid factors for all grains and for grains sharing cavity in sample deformed under T2 condition and** ***b*** **distribution of mean disorientation spread for all grains and for grains sharing 2GBVs as well as 3GBVs (sample T1)**

GB ledges,[3] which can be grown in features at GBs or induced by plastic deformation. According to this hypothesis, we expect that the sample deformed under T2 conditions experiencing more plastic slip than climb will contain more 2GBVs than the T1 sample. Indeed experimental data of Table 1 confirm this assumption indicating a higher probability of 2GBVs in the T2 sample (8·3%) compared to the T1 sample (5·9%). It is important to emphasise that the contrary is observed for the probability of finding a void at a triple junction. The relative frequency of 3GBVs in the T1 sample is 4·0%, the double of the value observed under T2 conditions (1·9%). The difference should be related to the increased contribution of GBS, which augments with decreasing stress.[25] The same trend was observed for 4GBs, of which 91% are damaged in the T1 sample.

Finally, we emphasise that the higher volume of 3GBVs compared to 2GBVs in both samples (Fig. 5*b*), expected to be related to the mechanisms of void growth, might also be influenced by void coalescence. Since triple junction voids are in contact with more GBs, indeed all creep mechanisms such as creep plasticity, GB diffusion and GBS will be more effective due to an increased number of paths towards the void surface. This leads in the case of the T1 sample to an increased volume fraction of the less numerous 3GBVs (0·124%), which exceeds that of the more numerous 2GBVs (0·098%). To reduce the effect of coalescence, only voids with a size smaller than the mean grain size were considered in the analysis. This criterion excluded taking into account the small cracks visible in Fig 3.

Conclusion

Based on an improved serial sectioning method combining surface profilometry, SEM imaging and EBSD the 3D granular and damage structure of two creep deformed copper specimens was reconstructed. Three GB types were identified together with their probability of forming creep voids. The analysis has shown that:

1. Creep damage is determined by GB topology. The weakest locations in the polycrystal are the 4GBs, almost all being damaged in both samples.

2. The relative proportion of 2GBVs is higher than that of 3GBVs and increases with increasing stress. This suggests that in pure metals void nucleation is linked to GB ledges. There is a higher probability of finding a void near grains with higher GND density, emphasising the role of plasticity in void nucleation (probably through ledge formation).

3. The relative frequency of 3GBVs and 4GBVs increases with decreasing stress, highlighting the importance of GBS in void nucleation at triple and quadruple boundaries.

4. No correlation between void location and the crystallographic orientation (Schmid factor) of neighbour grains was found.

The present experimental results and conclusions reveal the role of GB topology and GB faults on creep void nucleation. As the results describe only two copper samples, further investigations ensuring the generality of the present findings for pure metals are needed.

Acknowledgements

The authors acknowledge the help of the electron microscopy laboratory staff at EMSE, Sergio Sao-Joao and Marilyne Mondon. They also acknowledge the fruitful discussions and the comments of their colleague J. H. Driver.

References

1. M. F. Ashby and C. Gandhi: 'Taplin DMR Overview No. 3: Fracture-mechanism maps and their construction for f.c.c. metals and alloys', *Acta Metall.*, 1979, **27**, 699–729.
2. A. C. F. Cocks and M. F. Ashby: 'On creep fracture by void growth', *Prog. Mater. Sci.*, 1982, **27**, 189–244.
3. H. Riedel: 'Fracture at high temperatures'; 1987, Berlin/Heidelberg, Springer.
4. M. E. Kassner and T. A. Hayes: 'Creep cavitation in metals', *Int. J. Plast.*, 2003, **19**, 1715–1748.
5. A. R. Pyzalla, B. Camin, Th. Buslaps, M. Di Michiel, H. Kaminski, A. Kottar, A. Pernack and W. Reimers: 'Simultaneous tomography and diffraction analysis of creep damage', *Science*, 2005, **305**, 92–95.
6. J. Banhart, A. Borbély, K. Dzieciol, F. Garcia-Moreno, I. Manke, N. Kardjilov, A. R. Kaysser-Pyzalla, M. Strobl and W. Treimer: 'X-ray and neutron imaging – complementary techniques for materials science and engineering', *Int. J. Mater. Res.*, 2010, **101**, 1069–1079.
7. A. Isaac, F. Sket, W. Reimers, B. Camin, G. Sauthoff and A. R. Pyzalla: '*In situ* 3D quantification of the evolution of creep cavity size, shape, and spatial orientation using synchrotron X-ray tomography', *Mater. Sci. Eng. A*, 2008, **A478**, 108–118.
8. G. Requena, P. Cloetens, W. Altendorfer, C. Poletti, D. Tolnai and F. Warchomicka: 'Degischer HP sub-micrometer synchrotron tomography of multiphase metals using Kirkpatrick–Baez optics', *Scr. Mater.*, 2009, **61**, 760–763.
9. F. Sket, K. Dzieciol, A. Borbély, A. R. Kaysser-Pyzalla, K. Maile and R. Scheck: 'Microtomographic investigation of damage in E911 steel after long term creep', *Mater. Sci. Eng. A*, 2010, **A528**, 103–111.
10. K. S. Cheong, K. J. Stevens, Y. Suzuki, K. Uesugi and A. Takeuchi: 'The effects of microstructure on creep behaviour – a study through synchrotron X-ray tomography', *Mater. Sci. Eng. A*, 2009, **A513–A514**, 222–227.
11. K. Dzieciol, A. Borbély, F. Sket, A. Isaac, M. Di Michiel, P. Cloetens, T. Buslaps and A. R. Pyzalla: 'Void growth in copper during high-temperature power-law creep', *Acta Mater.*, 2011, **59**, 671–677.
12. A. Isaac, K. Dzieciol, F. Sket and A. Borbély: '*In-situ* microtomographic characterization of single-cavity growth during high-temperature creep of leaded brass', *Metall. Mater. Trans. A*, 2011, **42A**, 3022–3030.
13. B. Budiansky, J. W. Hutchinson and S. Slutsky: in 'Mechanics of solids', the R. Hill 60th anniversary volume, (ed. H. G. Hopkins and M. J. Sewell), 13; 1982, Oxford, Pergamon.
14. R. Marschallinger: 'A method for three-dimensional reconstruction of macroscopic features in geological materials', *Comput. Geosci.*. 1998, **24**, 875–883.
15. E. Schroeder-Reiter, F. Pérez-Willard, U. Zeile and G. Wanner: 'Focused ion beam (FIB) combined with high resolution scanning electron microscopy: a promising tool for 3D analysis of chromosome architecture', *J. Struct. Biol.*, 2009, **165**, 97–106.
16. M. Li, S. Ghosh, O. Richmond, H. Weiland and T. Rouns: 'Three dimensional characterization and modeling of particle reinforced metal matrix composites: part I', *Mater. Sci. Eng. A*, 1999, **A265**, 153–173.
17. K. M. Wu and M. Enomoto: 'Three-dimensional morphology of degenerate ferrite in an Fe–C–Mo alloy', *Scr. Mater.*, 2002, **46**, 569–574.
18. N. Chawla, V. V. Ganesh and B. Wunsch: 'Three-dimensional microstructure visualization and finite element modeling of the mechanical behavior of SiC particle reinforced aluminum composites', *Scr. Mater.*, 2004, **51**, 161–165.
19. A. Borbély and A. R. Kaysser-Pyzalla: 'X-ray diffraction microscopy: emerging imaging techniques for nondestructive analysis of crystalline materials from the millimetre down to the nanometre scale', *J. Appl. Cryst.*, 2013, **46**, 295–296.
20. P. Reischig, A. King, L. Nervo, N. Viganó, Y. Guilhem, W. J. Palenstijn, K. J. Batenburg, M. Preuss and W. Ludwig: 'Advances in X-ray diffraction contrast tomography: flexibility in the setup geometry and application to multiphase materials', *J. Appl. Cryst.*, 2013, **46**, 297–311.
21. S. F. Li, J. Lind, C. M. Hefferan, R. Pokharel, U. Lienert, A. D. Rollett and R. M. Suter: 'Three-dimensional plastic response in

polycrystalline copper via near-field high-energy X-ray diffraction microscopy', *J. Appl. Cryst.*, 2012, **45**, 1098–1108.
22. A. A. Wahab and M. V. Kral: 'A three dimensional view of high temperature creep damage', *Mater. High Temp.*, 2007, **24**, 299–302.
23. C. Gupta, H. Toda, C. Schlacher, Y. Adachi, P. Mayr, C. Sommitsch, K. Uesugi, Y. Suzuki, A. Takeuchi and M. Kobayashi: 'Study of creep cavitation behavior in tempered martensitic steel using synchrotron micro-tomography and serial sectioning techniques', *Mater. Sci. Eng. A*, 2013, **A564**, 525–538.
24. H. J. Frost and M. F. Ashby: 'Deformation-mechanism maps: the plasticity and creep of metals and ceramics', 1st edn; 1982, Oxford/New York, Pergamon Press.
25. T. G. Langdon: 'Grain boundary sliding revisited: developments in sliding over four decades', *J. Mater. Sci.*, 2006, **41**, 597–609.
26. K. Dzieciol, R. Abbasi and A. Borbély: in preparation.
27. J. M. Steigerwald, S. P. Murarka and R. J. Gutmann: 'Chemical mechanical planarization of microelectronic materials'; 1997, New York, John Wiley.
28. E. J. Garboczi: 'Three-dimensional mathematical analysis of particle shape using X-ray tomography and spherical harmonics: application to aggregates used in concrete', *Cem. Concr. Res.*, 2002, **32**, 1621–1638.
29. J. K. Mackenzie: 'Second paper on statistics associated with the random disorientation of cubes', *Biometrica*, 1958, **45**, 229–240.
30. C. R. Chen, S. X. Li and Z. G. Wang: 'Characteristics of strain and resolved shear stress in a bicrystal with the grain boundary perpendicular to the tensile axis', *Mater. Sci. Eng. A*, 1998, **A247**, 15–22.
31. B. J. Cane and G. W. Greenwood: *Met. Sci.*, 1975, **9**, 55.
32. P. J. Worthington and E. Smith: 'The formation of slip bands in polycrystalline 3% silicon iron in the pre-yield microstrain region', *Acta Metall.*, 1964, **12**, 1277–1281.
33. R. Raj and M. F. Ashby: 'Intergranular fracture at elevated temperature', *Acta Metall.*, 1975, **23**, 653–666.
34. V. Tvergaard and J. W. Hutchinson: 'Microcracking in ceramics induced by thermal expansion or elastic anisotropy', *J. Am. Ceram. Soc.*, 1988, **71**, 157–166.
35. C. W. Lau, A. S. Argon and F. A. McClintock: 'Stress concentrations due to sliding grain boundaries in creeping alloys', *Am. Soc. Test. Mater.*, 1984, **1**, 551–572.